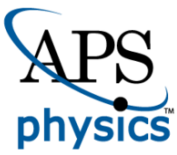

Stability of Dirac Liquids with Strong Coulomb Interaction

Igor S. Tupitsyn and Nikolay V. Prokof'ev

Phys. Rev. Lett. **118**, 026403 — Published 12 January 2017

DOI: 10.1103/PhysRevLett.118.026403

Stability of Dirac Liquids with Strong Coulomb Interaction

Igor S. Tupitsyn[1, 2] and Nikolay V. Prokof'ev[1, 2, 3]

[1]*Department of Physics, University of Massachusetts, Amherst, MA 01003, USA*
[2]*National Research Center "Kurchatov Institute", 123182 Moscow, Russia*
[3]*Department of Theoretical Physics, The Royal Institute of Technology, Stockholm SE-10691 Sweden*

(Dated: November 18, 2016)

We develop and apply the Diagrammatic Monte Carlo technique to address the problem of stability of the Dirac liquid state (in a graphene type system) against strong long-range part of the Coulomb interaction. So far, all attempts to deal with this problem in the field-theoretical framework were limited either to perturbative or RPA and FRG treatments, with diametrically opposite conclusions. Our calculations aim at the approximations-free solution with controlled accuracy by computing vertex corrections from higher-order skeleton diagrams and establishing the renormalization group flow of the effective Coulomb coupling constant. We unambiguously show that with increasing the system size L (up to $ln(L) \sim 40$), the coupling constant always flows towards zero; i.e. the two dimensional Dirac liquid is an asymptotically free $T = 0$ state with divergent Fermi velocity.

PACS numbers: 73.22.Pr, 71.30.+h, 05.10.Cc, 05.10.Ln

The linear in momentum low-energy part of electronic spectrum with vanishing density of states at the Fermi points in the undoped graphene results in a picture of massless two-dimensional (2D) Dirac fermions in a semimetallic state. While conventional 3D metals efficiently screen long-range Coulomb interactions and fall under the standard Fermi liquid description, 2D Dirac fermions leave Coulomb interactions unscreened. This, in turn, leads to a divergent renormalization of quasiparticle properties [1, 2], and the system is commonly referred to as the Dirac liquid (DL).

The effect of long-range Coulomb interactions (unrelated to the transition to the AFM insulator state with spontaneously broken chiral sublattice symmetry [3] caused by strong on-site repulsion) on properties of DL has been addressed theoretically in a number of works using both analytic and numeric approaches (see [1] and references therein). Within the lowest-order perturbation theory (Fock diagram) [4] it was found that the effective coupling constant $\alpha = e^2/\epsilon_0 v_F$ (where e is the electron charge, ϵ_0 is the background dielectric constant, and v_F is the Fermi velocity) renormalizes to zero logarithmically as the system size L is increased

$$d\alpha(l)/dl = -\alpha^2(l)/4\,, \quad l = \ln(L/a)\,. \tag{1}$$

Here a is the lattice constant (see Fig.1(a)). In the absence of charge renormalization [4, 5] this is equivalent to divergent renormalization group (RG) flow for the Fermi velocity $dv_F(l)/dl = \alpha v_F/4 = const$; i.e., the theory is asymptotically free if the bare coupling constant $\alpha_0 = e^2/\epsilon_0 v_F^{(0)}$ is small ($v_F^{(0)} = \sqrt{3}\,at/2$ is the Fermi velocity in the non-interacting system).

However, in suspended graphene the bare Coulomb coupling constant is not small, $\alpha_0 = 2.2$. When the RG equation for v_F is computed up to the next-to-leading order in α, it is found that the flow features an unstable infrared fixed point [6]. At this level of approximation,

$$dv_F/dl = [1 - c\alpha]\,\alpha v_F/4\,, \quad c \approx 1.2\,. \tag{2}$$

and the flow is towards strong coupling if $\alpha_0 > \alpha_c \approx 0.8$. On the one hand, this result hints at the possibility that DL may be unstable against strong Coulomb interactions. On the other hand, the value of α_c is not small and the second-order perturbative result cannot be trusted. Indeed, when the second-order calculation is upgraded to include an infinite sum of bubble diagrams (the so-called RPA approximation) the unstable infrared point is removed [7–9]; the same conclusion was reached within the functional renormalization group approach [10]. However, given that for $\alpha \geq 1$ all quantities are strongly renormalized, unaccounted (higher-order) diagrammatic contributions may alter the final result, leaving the question of stability of DL for strong Coulomb interactions an unsolved theoretical problem.

It should be mentioned that suspended undoped graphene is a semimetal, and significant enhancement of the Fermi velocity observed in measurements of the cyclotron mass [11] and ARPES spectra [12] indicates that we are dealing with stable DL. Early Hybrid Monte Carlo simulations [13–15] of the effective two-band model of graphene [16] with strong on-site repulsion and $\alpha_0 v_F^{(0)}/r$ Coulomb term at large distances predicted an insulating state for $\alpha_0 > 1$, in line with (2) and in contradiction with experiments. However, when a more realistic parametrization of inter-particle interactions at short distances was introduced [17, 18], suspended graphene was found to remain semimetallic. These results show that one has to be extremely careful in separating physics of strong short-range correlations from the RG flow due to long-range forces. Unfortunately, the largest system sizes simulated in Ref. [17] ($L/2a \leq 12$) were too small for constructing the RG flow of the effective Coulomb coupling.

To understand the role of strong long-range Coulomb

forces in a 2D Dirac liquid, similarly to what is done in effective field theories with an ultraviolet cutoff $\Lambda = 1/\xi$, one has to consider models that at length scales $\xi \gg a$ emerge as Dirac liquids with some effective coupling constant α, and study the RG flow of α at length scales $L \gg \xi$. Two observations immediately follow from this setup: (i) to achieve the goal one needs to consider large system sizes that satisfy both inequalities, i.e. $L \gg \xi \gg a$; (ii) simulations of models that show strong dependence of final results on contact terms are not suitable for this type of analysis because they either fail to produce Dirac liquid states at large scales or the corresponding cutoff scale ξ exceeds available system sizes L.

In this Letter we develop the bold-line Diagrammatic Monte Carlo (BDMC) technique for graphene type systems that allows us to deal with Coulomb interactions in a fully self-consistent, approximations free, manner and obtain final results with controlled accuracy by accounting for vertex corrections from higher-order skeleton diagrams. To demonstrate that BDMC leads to an accurate solution, we first benchmark the technique against a much harder (as far as the diagrammatic series are concerned) problem of the semimetal–insulator transition in suspended graphene by comparing our results with Refs. [17, 18]. The main topic of this study, however, is stability of DL against the strong long-range part of the Coulomb interaction, and we were able to establish the RG flow of the effective coupling constant over twelve(!) orders of magnitude in length scales. We find that the system always flows to the asymptotically free DL state (to suppress short-range correlations the interatomic potential is made constant at distances $r \leq 2a$). The proper solution of the problem does require that higher-order vertex corrections are accounted for in a fully self-consistent way because they significantly renormalize the flow at strong coupling.

System. Carbon atoms in graphene are arranged in a honeycomb lattice that can be seen as two identical triangular sublattices, $\mathbf{A}$ and $\mathbf{B}$, with unit vectors $\{\mathbf{a}_1, \mathbf{a}_2\}$, shifted relative to each other by $\mathbf{b} = (\mathbf{a}_1 + \mathbf{a}_2)/3$, see Fig.1(a). In what follows we use a as a unit of length. The Hamiltonian $H = H_0 + H_{\rm int}$ is defined by

$$H_0 = -t \sum_{<\mathbf{ij}>\sigma} (a^\dagger_{\mathbf{i}\sigma}\, b_{\mathbf{j}\sigma} + h.c.) - \mu \sum_{\mathbf{i}\sigma} n_{\mathbf{i}\sigma} \qquad (3)$$

$$H_{\rm int} = \frac{1}{2} \sum_{\mathbf{ij}\sigma\sigma'} V_{\sigma\sigma'}(|\mathbf{r_i} - \mathbf{r_j}|)\, n_{\mathbf{i}\sigma} n_{\mathbf{j}\sigma'}\,, \qquad (4)$$

where H_0 is based on the standard tight-binding approximation characterized by the nearest-neighbor (between sublattices) hopping amplitude t and chemical potential μ. [BDMC technique can deal with arbitrary lattice dispersion relation.] The second term describes electron-electron interactions with the Coulomb-law form at large distances (we employ standard second-quantization notations for creation, annihilation, and density operators in the site representation). The on-site coupling, $V_{\sigma\sigma'}(0) = U\delta_{\sigma,-\sigma'}$, is the only interaction term that depends on the spin index $\sigma = \pm$; all other couplings are spin-independent, $V_{\sigma\sigma'}(r > 0) = V_c(r)$ with $V_c(r >> a) \to e^2/\epsilon_0\, r$.

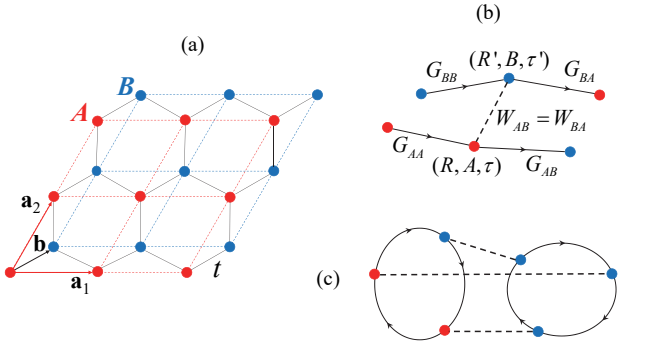

FIG. 1: (color online). (a) Honeycomb lattice of graphene with the nearest-neighbor hopping amplitude t ($|\mathbf{a}_1| = |\mathbf{a}_2| = a$). (b) The basic building block for the G^2W skeleton expansion is based on three-point vertexes characterized by the unit cell index $\mathbf{R}$, imaginary time τ, and sublattice index $\xi = \{\mathbf{A}, \mathbf{B}\}$. Green's functions G and screened interactions W are connecting three-point vertexes pairwise. (c) Typical skeleton free-energy diagram.

Formalism. Our calculations are based on the standard Feynman diagrammatic technique re-formulated in terms of the self-consistent G^2W skeleton expansion [19]. In the real-space imaginary-time representation the free-energy skeleton diagrams are composed of three-point vertexes located at space-time positions $(\mathbf{r}, \tau)$ and connected pairwise by fully-dressed Green's functions, G, and screened effective interactions, W, see Fig. 1(b), in such a way that the resulting graph is (i) connected, (ii) cannot be made disconnected by cutting two lines of the same kind, see Fig. 1(c). The only exception is the Hartree diagram, which can be absorbed into the chemical potential (in general, spin and sublattice dependent).

Within the BDMC framework (see Refs. [20, 21] for more details), the configuration space of skeleton diagrams for free-energy is sampled stochastically; by removing one of the graph lines, either G or W, one obtains a diagram either for the proper electron self-energy Σ or irreducible polarization function Π. The self-consistency loop is closed by Dyson equations that take an algebraic form in the momentum-frequency space:

$$G^{-1} = G_0^{-1} - \Sigma\,, \qquad W^{-1} = V^{-1} - \Pi\,. \qquad (5)$$

For brevity, we do not explicitly mention the tensor structure of interactions, propagators, and irreducible objects in the sublattice and spin space. On a honeycomb lattice all quantities are 2×2 matrices in the basis $|\phi_\xi(\mathbf{R})\rangle$, where $\xi = \{\mathbf{A}, \mathbf{B}\}$ and $\mathbf{R}$ is the unit cell index. In this basis, the bare Green's function is given by $(G_0)_{\xi\xi'}(\mathbf{R} - \mathbf{R}') = \sum_\gamma \langle\phi_\xi(\mathbf{R})|\Phi_\gamma\rangle (G_0)_\gamma \langle\Phi_\gamma|\phi_{\xi'}(\mathbf{R}')\rangle$ with $(G_0)_\gamma = (i\omega_n + \mu - \epsilon_s(\mathbf{k}))^{-1}$, where $|\Phi_\gamma\rangle$ is the

$\gamma = (s, \mathbf{k})$-th eigenstate of the tight-binding Hamiltonian with eigenenergy $\epsilon_{s=1,2}(\mathbf{k})$ and $\omega_n = 2\pi T(n + 1/2)$ with integer n is the fermionic Matsubara frequency.

Our implementation of the BDMC technique, generalized to several atoms in the unit cell, closely follows that of Ref. [20]. Both Σ and Π are computed as sums of all skeleton graphs up to order N (there are $2N$ vertexes in the N-th order graph); we denote these sums as Σ_N and Π_N. The lowest-order contributions Σ_1 and Π_1 are nothing but products of G and W functions, and at $N = 1$ the scheme is identical to the GW-approximation. Monte Carlo statistics has to be collected only from higher-order diagrams. The skeleton formulation is complete and the diagrammatic sequence for long-range Coulomb interactions on a lattice is expected to converge with increasing the diagram order [21]. The largest system size considered in this work was $L^2 = 256^2$ (the number of atoms/sites is $2L^2$), with periodic boundary conditions.

Semimetal-insulator transition. To demonstrate how the BDMC technique works and what expansion orders lead to accurate results, we benchmark it against the semimetal - insulator (AFM) transition problem in suspended undoped ($n_e = 1$) graphene. Following Ref. [17] we introduce the "chiral" symmetry breaking term

$$H_{SB} = h \left(\sum_{\mathbf{i} \in \mathbf{A}} m_{\mathbf{i}} - \sum_{\mathbf{j} \in \mathbf{B}} m_{\mathbf{j}} \right) , \qquad (6)$$

where $m_{\mathbf{i}} = \sum_\sigma \sigma n_{\mathbf{i}\sigma}$ is the spin density operator. [In Hybrid Monte Carlo this term is required to remove zero modes in the fermionic sector [18]; here we add it solely for the purpose of exact comparison.] The order parameter is defined as the difference between the sublattice magnetizations: $\Delta m = m_{\mathbf{A}} - m_{\mathbf{B}}$. It goes to zero when $h \to 0$ in the semimetal and saturates to a finite value in the gapped AFM phase.

Simulations in Ref. [17] were done for $t = 2.7$, at $T = 0.5$ (we use eV as the unit of energy). Screening by σ-band electrons was accounted for by adjusting on-site and n.n, n.n.n., and n.n.n.n coupling constants to the result of the constrained RPA calculation [22]: they were set to 9.3, 5.5, 4.1, and 3.6, respectively. At larger distances the long-range Coulomb potential was added as $V(r > 2a/\sqrt{3}) = 7.2\, a/\sqrt{3}r$ (for details see [17, 22]). The order parameter was evaluated for $h = 0.1, 0.2, \ldots$. We consider exactly the same parameter sets.

In Fig.2 we compare Hybrid Monte Carlo data for Δm to BDMC results obtained from the skeleton expansion truncated at order $N = 1, 2, 3, 4$. We observe that regardless of the value of h the skeleton series converge, and $N = 3, 4$ results are indistinguishable from results reported in Refs. [17, 18] within their error bars. We also performed calculations with the scaled, $V(r) \to V(r)/\bar{\epsilon}$, potential (results for $\bar{\epsilon} = 0.65$ are not shown here for brevity). We confirm that gap opening takes place at $\bar{\epsilon} \sim 0.7$. This test ensures that the BDMC scheme is capable of capturing all important electronic correlations even in close vicinity of the semimetal-insulator transition. While the GW approximation ($N = 1$) is rather unsatisfactory in this strongly correlated regime, excellent accuracy can be reached by extending the skeleton calculation up to order $N = 3$.

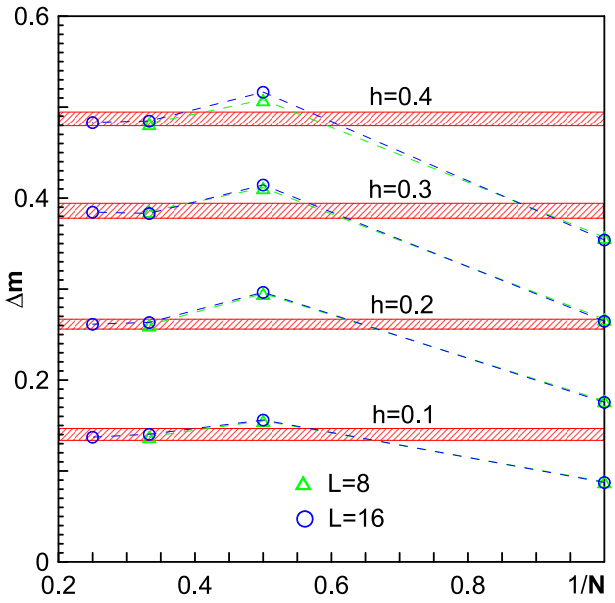

FIG. 2: (color online). The order parameter Δm as a function of inverse skeleton order $1/N$. Calculations were performed for system sizes $L = 8$ (green triangles) and 16 (blue circles) and for different values of the symmetry breaking field $h = 0.1, 0.2, 0.3, 0.4$. By filled red stripes we show the corresponding results (with error bounds) from Ref. [17] for $L = 18$.

Dirac liquid. We now focus on the main result of this work: the RG flow of the effective Coulomb coupling α in DL described by Eqs. (3) and (4). Suppressing short-range correlations by making the interaction potential flat over some finite scale is very important for revealing effects due to long-range forces. Otherwise, it would be impossible to study large values of α_0 because of the semimetal-insulator transition taking place for unrelated reasons.

To construct the RG flow for $\alpha(l) = \alpha_0 v_F^{(0)}/v_F$ we compute Fermi velocities in systems with different linear sizes L at temperatures lower than the energy of the first excited state $T \lesssim \min\{|\epsilon_{s\mathbf{k}} - \mu|\} \propto L^{-1}$. This is done by standard analysis of the singular part of the Green's function at the Dirac point $\mathbf{K}$. We start by obtaining eigenvectors of the $\tilde{H} = H_0 + \mathrm{Re}\Sigma$ operator evaluated at zero frequency ($\tilde{H}$ is a 2×2 matrix in the sublattice space for every momentum; the spin index plays no role here and is suppressed). The corresponding eigenvalues are denoted as $\tilde{\epsilon}_{s=1,2}(\mathbf{k})$. After rotating $[1 - \mathrm{Im}\Sigma(\mathbf{K}, \omega_n)/\omega_n]^{-1}_{\omega_n \to 0}$ matrix to the basis of obtained eigenvectors, we get the quasiparticle residue Z from its diagonal elements (non-diagonal elements are zero with high accuracy), and de-

termine the Fermi velocity from $v_F = Z[d\tilde{\epsilon}_s(\mathbf{k})/dk]_{\mathbf{k}\to\mathbf{K}}$.

In Fig. 3 we present results obtained within the $N = 1$, or GW, approximation for system sizes $L = 16, 32, 64, 128$, and 256 and a number of bare coupling constants (smaller system sizes are disregarded to minimize the role of short-range correlations). In all cases we find that α always decreases with the system size, indicating that there is no unstable infrared point at $\alpha \sim 1$. However, individual curves account only for a moderate amount of renormalization and do not allow one to relate strong to weak coupling limits by the RG flow. This deficiency is eliminated by employing the flowgram method developed in Ref. [23].

The single-parameter flowgram idea is based on the assumption (to be verified by the data) that the flow at large scales is of the form (below $\{L, \xi\} >> a$)

$$\alpha(L)/\alpha(\xi) = F[L/\xi]\,, \quad F(0) = 1\,, \tag{7}$$

where $F(x)$ is a universal function, and all dependence on microscopic parameters is absorbed into the definition of the length scale ξ. If this assumption is correct, then $[d\alpha/dl]/\alpha(\xi)$ is a universal function of L/ξ; i.e., the flow derivatives (and thus the entire flow) for different microscopic Hamiltonians have to coincide if values of α are matched at some large length scale. For the logarithmic variable $l = \ln(L/\xi)$, selecting a different length scale ξ is equivalent to shifting the flow curve horizontally.

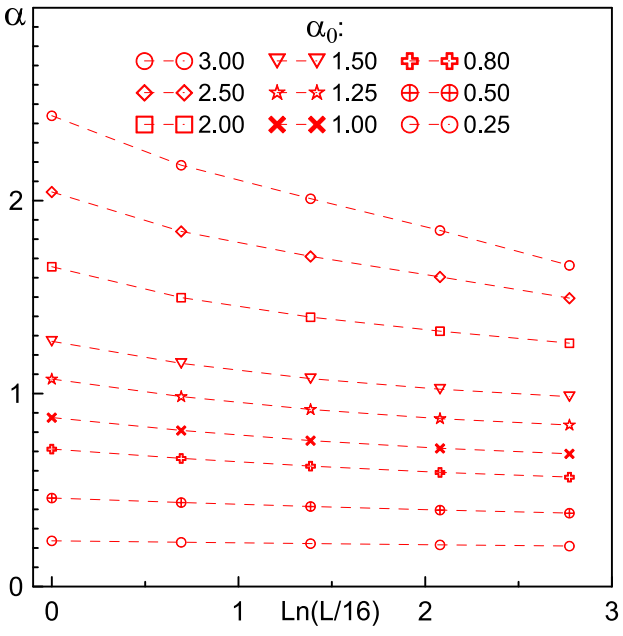

FIG. 3: (color online). RG flow of α with system size for various bare coupling constants α_0 within the GW approximation.

This consideration leads to the following procedure of constructing the RG flow shown in Fig. 4. We start with data shown in Fig. 3 and for each value of α_0 we translate the corresponding flow curve along the x-axis until $\alpha(\alpha_0, L = 64)$ data overlap with the data for larger value of α_0 at larger L. Since there is no freedom in adjusting local derivatives, the scaling hypothesis (7) is confirmed because all data for large enough L collapse on a single smooth master curve. The result is a flow from strong to weak coupling that effectively extends over twelve (!) orders of magnitude.

After establishing the RG flow in the *GW* approximation, we repeat the above analysis for higher-order skeleton formulations with $N = 2$ and $N = 3$. Since these computations are more demanding they were mostly limited to $L = 32$ and 64 (and $L = 128$ for smaller values of α_0 at $N = 2$). The protocol of constructing the master curves for $N = 2,\ 3$ is exactly the same as for $N = 1$, i.e. it is obtained by shifting flow curves horizontally. The result is shown in Fig. 4. Clearly, the effect of vertex corrections is very pronounced for $\alpha > 1$, but the skeleton sequence quickly converges and $N = 3$ results are nearly identical to those for $N = 2$. The final flow is always to the asymptotically free DL with logarithmically divergent Fermi velocity and finite quasiparticle residue.

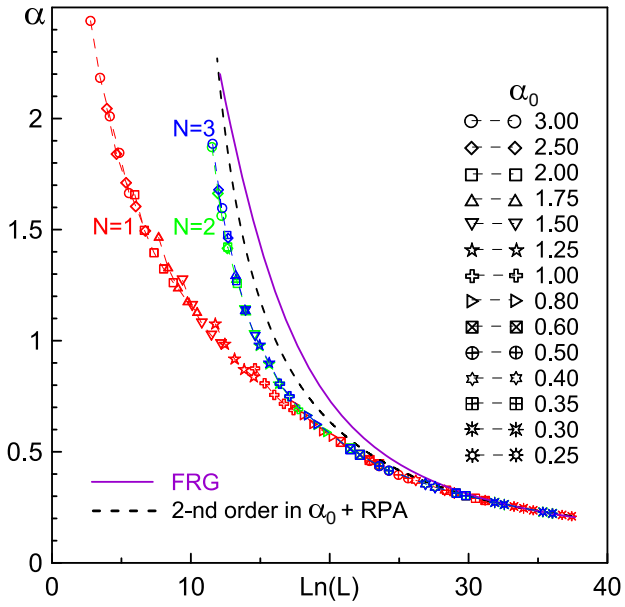

FIG. 4: (color online). RG flow of α with system size for $N = 1$ (red), $N = 2$ (green), and $N = 3$ (blue). GW curves were obtained for $L = 16, 32, 64, 128, 256$; for $L = 16$ there are visible deviations from the master curve because this size is not in the scaling limit yet. Curves for $N = 2$ and 3 were obtained for $L = 32, 64$, and 128 (see text). Black dashed line is the RG flow based on the second-order+RPA approximation [1, 7, 8]. Purple solid line (courtesy of A. Sharma and P. Kopietz) is the flow obtained within the functional renormalization group approach [10].

Conclusions. We address the fundamental problem of the Dirac liquid stability against strong Coulomb interactions using the Diagrammatic Monte Carlo method that allows us to account for higher-order vertex corrections within the fully self-consistent skeleton expansion. We

find that even in the strongly correlated Dirac liquid the skeleton sequence quickly converges and leads to an accurate solution of the RG flow for the effective coupling constant. The unstable infrared point at $\alpha \approx 1$ is ruled out, and the flow is found to be always to the asymptotically free state.

Our approach is general and can be applied to any graphene-type system with arbitrary dispersion relation featuring Dirac cones, both doped and undoped, and with arbitrary shape of the interaction potential. Given that long-range electron-ion interactions in these systems are of the same Coulomb origin, future work should address them as well to achieve the best effective description of realistic materials.

Acknowledgements. We thank B. Svistunov for discussions. This work was supported by the Simons Collaboration on the Many Electron Problem, the National Science Foundation under the grant PHY-1314735, the MURI Program "New Quantum Phases of Matter" from AFOSR, the Stiftelsen Olle Engkvist Byggmästare Foundation, and the Swedish Research Council grant 642-2013-7837.

[1] V.N. Kotov, B. Uchoa, V.M. Pereira, F. Guinea, and A. H. Castro Neto, Rev. Mod. Phys. **84**, 1067 (2012).
[2] S. Das Sarma, E.H. Hwang, and Wang-Kong Tse, Phys. Rev. **B 75**, 121406(R) (2007).
[3] G.W. Semenoff, Phys. Rev. Lett. 53, 2449 (1984). Phys. Rev. **B 89**, 195429 (2014).
[4] J. Gonzâlez, F. Guinea, and M.A.H. Vozmediano, Nucl. Phys. **B 424**, 595 (1994).
[5] J. Ye and S. Sachdev, Phys. Rev. Lett. **80**, 5409 (1998).
[6] O. Vafek and M.J. Case, Phys. Rev. **B 77**, 033410 (2008).
[7] J. Gonzâlez, F. Guinea, and M.A.H. Vozmediano, Phys. Rev. **B 59**, R2474 (1999).
[8] D.T. Son, Phys. Rev. **B 75**, 235423 (2007).
[9] J. Hofmann, E. Barnes, and S. Das Sarma, Phys. Rev. Lett. **113**, 105502 (2014).
[10] A. Sharma and P. Kopietz, Phys. Rev **B 93**, 235425 (2016).
[11] D.C. Elias, R.V. Gorbachev, A.S. Mayorov, S.V. Morozov, A.A. Zhukov, P. Blake, L.A. Ponomarenko, I.V. Grigorieva, K.S. Novoselov, F. Guinea, and A.K. Geim, Nature Phys. **7**, 701 (2011); A.S. Mayorov, D.C. Elias, I.S. Mukhin, S.V. Morozov, L.A. Ponomarenko, K.S. Novoselov, A.K. Geim, and R.V. Gorbachev, Nano Lett. **12**, 4629 (2012).
[12] D.A. Siegel, C.-H. Park, C. Hwang, J. Deslippe, A.V. Fedorov, S.G. Louie, and A. Lanzara, Proc. Natl. Acad. Sci., **108**, 11365 (2011).
[13] J.E. Drut and T.A. Lähde, Phys. Rev. Lett. **102**, 026802 (2009); Phys. Rev. **B 79**, 241405 (2009).
[14] W. Armour, S. Hands and C. Strouthos, Phys. Rev. **B 81**, 125105 (2010).
[15] P. V. Buividovich and M. I. Polikarpov, Phys. Rev. **B 86**, 245117 (2012).
[16] I. Herbut, Phys. Rev. Lett. **97**, 146401 (2006).
[17] M. V. Ulybyshev, P. V. Buividovich, M. I. Katsnelson, and M. I. Polikarpov, Phys. Rev. Lett. **111**, 056801 (2013).
[18] D. Smith and L. von Smekal, Phys. Rev. **B 89**, 195429 (2014).
[19] L. Hedin, Phys. Rev. **139**, A796 (1965).
[20] S. A. Kulagin, N. Prokof'ev, O. A. Starykh, B. V. Svistunov, and C. N. Varney, Phys. Rev. Lett. 110, 070601 (2013); Phys. Rev. **B 87**, 024407 (2013).
[21] I.S. Tupitsyn, A.S. Mishchenko, N. Nagaosa, N. Prokof'ev, Phys. Rev. **B 94**, 155145 (2016).
[22] T.O. Wehling, E. Sasioglu, C. Friedrich, A.I. Lichtenstein, M.I. Katsnelson, and S. Blgel, Phys. Rev. Lett. **106**, 236805 (2011).
[23] A.B. Kuklov, M. Matsumoto, N.V. Prokof'ev, B.V. Svistunov, and M. Troyer, Phys. Rev Lett. **101**, 050405 (2008).